ELSEVIER

Urologic Oncology: Seminars and Original Investigations 29 (2011) 411–420

UROLOGIC ONCOLOGY

Original article

# Investigation of hypoxia and carbonic anhydrase IX expression in a renal cell carcinoma xenograft model with oxygen tension measurements and $^{124}$I-cG250 PET/CT☆

Nathan Lawrentschuk, F.R.A.C.S.[a,b,*], Fook T. Lee, Ph.D.[b], Gareth Jones, B.Sc (Hons)[c], Angela Rigopoulos, M.Sc.[b], Angela Mountain, B.App.Sci.[b], Graeme O'Keefe, Ph.D.[c], Anthony T. Papenfuss, Ph.D.[e], Damien M. Bolton, M.D.[a], Ian D. Davis, Ph.D.[b,d], Andrew M. Scott, M.D.[b,c,d]

[a] *University of Melbourne Department of Surgery, Austin Hospital, Melbourne, Victoria, Australia*
[b] *Ludwig Institute for Cancer Research, Tumor Targeting Laboratory, Austin Hospital, Melbourne, Victoria, Australia*
[c] *Centre for Positron Emission Tomography, Austin Hospital, Melbourne, Victoria, Australia*
[d] *University of Melbourne Department of Medicine, Austin Hospital, Melbourne, Victoria, Australia*
[e] *Walter and Eliza Hall Institute of Medical Research, Melbourne, Victoria, Australia*

Received 2 March 2009; received in revised form 26 March 2009; accepted 31 March 2009

**Abstract**

**Objectives:** In tumors, hypoxia stimulates angiogenesis and correlates with treatment resistance and poor prognosis. We have previously demonstrated hypoxia in human renal cell carcinoma (RCC) via direct oxygen probe measurements. Carbonic anhydrase IX (CA IX) is a protein stimulated by hypoxia and involved in angiogenesis, and is a potential tumor target for imaging and therapies using cG250, a monoclonal antibody that recognizes CAIX. Our objectives were to characterize intratumoral hypoxia in a human RCC xenograft model using oxygen probe measurements; investigate if $^{124}$I-cG250 targets RCC correlating uptake on noninvasive positron emission tomography-computerized tomography (PET-CT) against traditional biodistribution studies, and investigate CAIX expression in this RCC model.

**Methods:** BALB/c nude mice had human RCC (SK-RC-52) subcutaneously xenografted with oxygen levels measured by probe. Positron emission tomography (PET/CT) and biodistribution studies ($^{124}$I-cG250) were correlated with oxygen measurements. Immunohistochemistry and autoradiography were performed on selected tumors to confirm CAIX expression

**Results:** Oxygen tension in normal tissue (muscle) was 35.08 ± 2.41 mmHg (mean ± 95% CI), significantly greater compared to xenograft SK-RC-52 tumors at 5.02 ± 1.12 mmHg. Biodistribution studies of $^{124}$I-cG250 demonstrated isotope uptake in SK-RC-52 xenografts peaking at 23.45 ± 5.07% ID/g (mean ± SD) 48 hours after antibody injection, which was maintained for a further 2 days (19.43 ± 4.31 and 10.64 ± 5.64 % ID/g, respectively). PET studies demonstrated excellent localization of $^{124}$I-cG250 in tumor, and a significant correlation between SUVmean, SUVmax, and %/ID $^{124}$I-cG250. CAIX expression was present in all groups studied but there was no significant correlation between it and any oxygen parameter studied.

**Conclusion:** Intratumoral hypoxia does exist within a human RCC xenograft model using invasive oxygen probe measurements. $^{124}$I-cG250 targets RCC with correlation between uptake on noninvasive PET-CT studies and traditional biodistribution studies opening the possibility of using PET/CT in future studies. Finally, CAIX expression was not related to hypoxia in this model, supporting the hypothesis that cell lines may subvert known hypoxia mechanisms in hypoxic environments. 

*Keywords:* Renal neoplasms; Diagnostic imaging; Positron emission tomography; Radionuclide imaging; Radioimmunodetection; Antibodies monoclonal; Murine

## 1. Introduction

Patients with renal cell carcinoma (RCC) continue to present a therapeutic challenge despite improved treatment modalities [1]. Hypoxia is known to be a key factor responsible for tumor resistance to therapy in humans. This occurs

☆ Research was generously supported by the Melville Hughes Scholarship (N.L.), Faculty of Medicine Dentistry and Health Sciences, University of Melbourne, Australia.

* Corresponding author. Tel.: +61 3 9496 5669; fax: +61 3 9458 5023.
*E-mail address:* nathan.lawrentschuk@uhn.on.ca (N. Lawrentschuk).

1078-1439/$ – see front matter © 2011 Elsevier Inc. All rights reserved.
doi:10.1016/j.urolonc.2009.03.028

principally via resistance to radiation [2] and chemotherapeutic agents [3,4]. Invasive polarographic oxygen sensor measurements have demonstrated hypoxia (oxygen tension less than 10 mmHg) in solid tumors [5]. Perhaps of more importance is that hypoxia has been demonstrated to be a prognostic indicator for local control after treatment with radiotherapy in glioma, head and neck, and cervical cancers [6–8]. Hypoxia has also been able to predict for survival and the presence of distant metastases in soft tissue sarcomas [9]. Finally, the significance of hypoxia in the activation and induction of functional molecules, such as hypoxia inducible factors and vascular endothelial growth factor (VEGF), the modulation of gene expression (e.g., carbonic anhydrase IX), increased proto-oncogene levels, activation of nuclear factors, and accumulation of other proteins (e.g., TP53) has been reported, although is yet to be completely defined [10,11].

The G250 antigen has recently been identified as a transmembrane protein identical to the tumor-associated antigen MN or carbonic anhydrase IX (CA IX) [12]. CAIX is a membrane-associated carbonic anhydrase integral in the regulation of cell proliferation in response to hypoxic conditions and may be involved in oncogenesis and tumor progression [13]. The subcellular pathways responsible for changes with tumor hypoxia are complex but involve, at least in part, the expression of hypoxia inducible factors (e.g., HIF-1$\alpha$) and VEGF. Interestingly, a close correlation between HIF-1$\alpha$ expression and CAIX expression has been observed in RCC [14]. Further supporting the relationship between hypoxia and CAIX expression is that in RCC synthesis of CAIX is switched on by the loss of the tumor suppressor gene VHL, whose product is integral to the hypoxia-1$\alpha$ (HIF-1$\alpha$) pathway [15]. Links between hypoxia and CAIX expression in other tumors are being defined [16–18], and although hypoxia has only recently been demonstrated in RCC, relationships between hypoxia and CAIX have not been explored [19].

The monoclonal antibody (mAb) G250 recognizes CAIX, which is highly expressed on the cell surface of almost all RCC, but has restricted expression in normal tissues, with the exception of gastric mucosa and larger bile ducts [20]. The targeting of RCC expressing the G250 antigen has been studied with both murine and chimeric G250 mAb. The generation of a chimeric form of G250 (mouse Fv and human IG1 Fc refers to cG250) has also been performed, resulting in reduced immunogenicity of the murine G250, whilst retaining the antigen specificity for CAIX of the parent murine antibody that has been demonstrated with in vitro competitive binding studies with $^{131}$I targeting RCC [21,22]. Further studies on renal tumors demonstrated selective uptake of mAb G250 in CAIX antigen-positive cells vs. antigen-negative cells [13]. Tumor uptake of murine and chimeric G250 in human trials has been shown to be amongst the highest level of quantitative uptake demonstrated by any antibody in a solid tumor [21–23]. Supporting this is a recent clinical study using cG250 PET, which accurately identified 15 of 16 clear cell RCC whereas 9 non-clear-cell renal masses were negative for the tracer [24].

Therapeutic trials with chimeric G250 (cG250) as a naked antibody [22], in conjunction with cytokines [22] and for radioimmunotherapy [20,25] have been conducted, and have shown promise as targeting strategies and potential therapies for RCC. The identification of CAIX expression in tumors with radioimmunoscintigraphy using positron emitters (immuno-PET) linked to cG250 has the potential to define this important marker of hypoxia noninvasively. Characterization of intratumoral hypoxia using the "gold standard" of an invasive oxygen sensor probe xenograft human RCC models has not been performed previously, with only a murine RCC model studied in a very small cohort [26].

Direct data linking hypoxia and CAIX expression is lacking in RCC. On one hand, the hypothesis is that CAIX expression will reflect hypoxia given the pathways involved with loss of VHL. Another point of view is that the loss of VHL will enable tumors to subvert such pathways and that CAIX expression is not related to hypoxia, particularly in such models. Both arguments have merit.

Hence, the purpose of this study was therefore 3-fold:

(1) Characterize that intratumoral hypoxia exists in a human RCC xenograft model using invasive oxygen probe measurements.

(2) Investigate if 124I-cG250 targets tumors in a human RCC xenograft model and if there is a correlation between uptake with noninvasive PET-CT studies against traditional biodistribution studies, using $\gamma$ well counting. Such a finding could create alternative strategies in experimental design using fewer animals serially scanned rather than sacrificed at different time points.

(3) Investigate whether or not CAIX expression is related to hypoxia in this model. This is important, as many cell lines have subverted hypoxia mechanisms, and CAIX expression is not necessarily a result of hypoxia.

## 2. Materials and methods

### 2.1. mAbs

The generation and characterization of the original murine mAb cG250 and its humanization have been described previously [21,23]. cG250 (Wilex AG, Munich, Germany) was obtained, whilst humanized anti-A33 mAb (huA33), which specifically recognizes the A33 antigen of colon cancer and does not bind G250-expressing cells [27], was produced in the Biological Production Facility (Ludwig Institute for Cancer Research, Melbourne, Victoria, Australia).

### 2.2. Cell lines

SK-RC-52, a CAIX expressing human RCC cell Line [22] was obtained from the American Type Culture Collection (Rockville, MD). These lines are from a metastatic RCC and are consistent with a VHL mutated cell line [28]. Cells were grown in 175-$cm^2$ plastic flasks (Nunclon; Nunc, Roskilde, Denmark) and maintained in log-phase growth in RPMI 1640 (Trace Biosciences, Sydney, Australia) supplemented with 5% FCS (MultiSer; Trace Biosciences, Sydney, Australia), 100 units/ml penicillin, 100 mg/ml streptomycin, 0.25 ml/l insulin, 2 mM glutamine, and essential amino acids. Cells were cultured at 37°C in a 5% $CO_2$ incubator (Forma Scientific, Inc., Marietta, OH) and passaged with 0.05% EDTA/PBS (BDH Chemicals, Merck, Melbourne, Australia). Cell viability in all experiments, as determined by trypan blue exclusion, exceeded 90%.

### 2.3. Radiolabeling and quality assurance

All analytical grade reagents in the experiments described, except when stated, were obtained from Merck Pty. Ltd. (Melbourne, Australia). $^{124}I$ in 0.02 N NaOH [10 mCi/ml] was purchased from Advanced Nuclide Technologies (Voorhees, NJ). An aliquot of 0.18 ml 0.5 M potassium phosphate buffer, pH 7.5 was added to 0.09 ml of $^{124}I$ in 0.05N NaOH (1080 $\mu$Ci). Radioactivity was measured either with a dose calibrator, Biodex Atomlab-100 (Brookhaven, NY) or a shielded Cobra II automated gamma counter (Canberra-Packard, Melbourne, Australia). An aliquot of 0.15 ml of this mixture was added to 60 $\mu$l of cG250 antibody (5 mg/ml) followed by 2 iodogen glass coated beads. After 10.0 minutes, labeling mixture removed and purified on a 5 ml Sephadex G50 column equilibrated in saline. The control antibody hu A33 was similarly radiolabeled and purified [29]. Radiochemical purity of labeled antibody was analyzed by instant-thin layer chromatography-silica gel (ITLC-SG) using 10% wt/vol trichloroacetic acid as solvent. Radioactivity bound to antibody remains at the origin whereas free $^{124}I$ migrated with the solvent front. Radiolabeling was performed on the day of injection into mice. Radiochemical purity was assessed prior to injection with the percentage of unbound radionuclide content was determined by ITLC-SG developed using 10% TCA solution [30].

### 2.4. Immunoreactive assays and receptor expression

#### 2.4.1. Lindmo and Scatchard assays

The immunoreactivity of cG250 after radiolabeling was determined using the assay of Lindmo et al. [31]. This cell-based assay consisted of incubating 20 ng radiolabeled antibody with increasing concentrations of SK-RC-52 ranging from 0 to $6.0 \times 10^6$ cells in 1.0 ml medium. The cells were incubated for 45 minutes at room temperature with continuous mixing. After 45 minutes at room temperature, the cells were centrifuged and washed 3 times with medium to remove unbound antibody, and pellets were measured double spaced in a $\gamma$ counter (Cobra II Model 5002, Auto-$\gamma$; Canberra-Packard, Melbourne, Australia). Standards were measured at the same time as pellets, and percentage binding of radiolabeled cG250 to SK-RC-52 cells was calculated. The immunoreactivity was determined by plotting the double reciprocal plot for binding against cell concentration using GraphPad Prism 4.0 software (GraphPad Inc., San Diego, CA). Scatchard analysis was used to determine the affinity constant ($K_a$) and number of antigen binding sites/cell as previously described [32].

#### 2.4.2. Fluorescence-activated cell sorting (flow cytometry) of receptor expression

Cells were either left pure or incubated with primary antibody (cG250) or a negative control antibody (IgG1) for assessment of CAIX expression. Analysis was done using an Epics Elite ESP (Beckman Coulter, Hialeah, FL) by observing a minimum of 20,000 events and data analyzed using EXPO (ver. 2) for Windows.

#### 2.4.3. Serum stability

The stability of radioconjugates in the blood circulation of mice was also determined. Serum was obtained at days 0, 3, and 7 postinjection. An aliquot of serum was spotted on an ITLC-SG strip and developed using 10% wt/vol trichloracetic acid as solvent. For immunoreactivity assay, concentrations of radiolabeled antibody in mouse serum were estimated from the blood-time activity curve of the biodistribution study and used in the cell-binding assay.

### 2.5. Animal model

The SK-RC-52 human RCC xenograft model was established from a single tumor by serial subcutaneous transplantations in nude mice after implantation of cells from culture suspended in reconstituted basement membrane (Matrigel) as previously described [33,34]. Tumor pieces (approximately 2 mm [3]) were transplanted subcutaneously beneath the nuchal fold of 6 week-old athymic BALB/c, nu/nu mice (Animal Resources Centre, Perth, Australia). In vivo biodistribution, PET and direct oxygen tension studies were initiated 10 weeks after inoculation. Tumor volume was calculated by the formula [(length $\times$ width$^2$)/2], [35], where length was the longest axis and width the measurement at right angles to the length.

Food and water were provided for the mice ad libitum and their health was monitored daily. Mice were maintained in autoclaved microisolator cages housed in a positive pressure containment rack (Thoren Caging Systems, Inc., Hazelton, PA). Mice were identified by earmarks and were weighed weekly. Animal care and experiments followed the Australian Code of Practice for the Care and Use of Animals for Scientific Purposes endorsed by the National Health and Medical Research Council, and was approved by our institutional animal ethics committee.

### 2.6. Oxygen tension measurement

Tumor tissue oxygen tension measurement, PET/CT imaging, and biodistribution studies were performed 10 weeks after tumor induction, at which time the mice weighed 11–23 g. The oxygen tension was initially measured in groups of mice at different tumor volumes to establish the level of oxygenation within a RCC tumor model. A subsequent experiment was undertaken to further correlate oxygen tension with standard tissue biodistribution of radiolabeled mAb cG250 using traditional $\gamma$ well counting of harvested tissues, PET studies, and immunohistochemistry in the same RCC model as the first experiment. Thus, the methods were identical for the components of the experiments that were shared.

Tumor $pO_2$ was measured with a 2-channel time-resolved luminescence-based optical oxygen-sensing probe (Oxylite 2000; Oxford Optronix, Oxford, UK) or oxylite probe. The probes (230 um o.d.) were precalibrated by the manufacturer ($\pm 0.7$ mmHg or $< \pm 10\%$ of actual $pO_2$, whichever was greater). To further ensure correct $pO_2$ readings in the experiments, the probe was checked in normal saline, and again in animals just sacrificed to ensure a 0 mmHg recording as previously described [36,37]. Additionally, we conducted control measurements in the right leg muscle of each animal for comparison with tumor measurements.

Animals that had not been anesthetized for PET studies as outlined above had anesthetic administered prior to oxygen tension studies. Body core temperature was maintained in animals by a heated pad at 37.5°C. Tumor temperature was measured by a fine thermocouple that was attached to the oxylite probe giving automatic temperature compensation [38]. The probes were inserted into the periphery of the tumors, avoiding necrotic areas, by puncturing with a 23 gauge intravenous needle and inserting the oxylite probe retrograde into the sheath as per manufacturer recommendations. This ensured minimal tissue and probe trauma. The probe was then fixed with a micromanipulator and allowed to stabilize over several minutes as previously described to ensure quality readings [3]. Each tumor had 3 tracks with the probe and a minimum of 100 measurements, summarized via computer software (WinDaq Data Acquisition Software; DATAQ Instruments Inc., Akron, OH). Mice were killed by exposure to sevofluorane, and then dissected prior to $\gamma$ well counting for the biodistribution analysis as outlined above.

Recording of oxygen levels in tissues was done for the mean $pO_2$, hypoxic fraction (percentage of readings) less than or equal to 2.5 mmHg, ($HF_{2.5}$), 5 mmHg ($HF_5$), and 10 mmHg ($HF_{10}$). The first (day 0, $n = 5$) and last (day 14, $n = 5$) groups of tumors were analyzed in depth because of the increases in growth that occurred across the 2 weeks of the study potentially making them different. These were also the groups having immunohistochemistry for CAIX (see below).

### 2.7. PET/CT imaging

PET/CT imaging was performed in groups of 5 or 6 mice at the following time points: day 0 (2 hours), 1 (24 hours), 3, 7, and 10 after $^{124}$I-cG250 injections. All mice were injected with 5 MBq $^{124}$I-cG250 (25 $\mu$g) in 0.2 ml PBS on day 0. Mice then went on to have oxygen tension measurements and biodistribution studies within minutes of scan completion as described previously. Animals were anesthetized via intraperitoneal injection of xylocaine hydrochloride (20 mg/ml, Troy Laboratories Pty Ltd., Smithfield, Australia) and ketamine (100 mg/ml, Parnell Laboratories, Alexandria, Australia). Mice were positioned on a PET/CT (Gemini PET and Dual slice Philips MX 8000 CT; Philips Electronics North America Corporation, New York, NY). The CT images were obtained first (5 minutes) and then a 30-minute PET acquisition was performed using a three-dimensional (3D) acquisition mode. Measured attenuation correction was performed and images were reconstructed using a standard 3D reconstruction algorithm and the CT scans were used to guide drawing of regions of interest (ROIs) for standardized uptake value (SUV) analysis.

### 2.8. Pharmacokinetics

A 2-compartment model of the concentration of antibody ($^{124}$I-cG250) in serum, peripheral tissue, and tumor with bolus IV injection, no lag time and mixed macro- and micro-parameters was fitted to the measured concentration antibody from the serum and tumor compartments.

Fitting was performed by minimizing the sum of the weighted, squared residuals using the Nelder-Mead method of the general-purpose optimization function (optim) in statistical program R (version 2.2.0; The R Foundation for Statistical Computing, Madison, WI; http://www.r-project.org/).

### 2.9. Biodistribution

cG250 biodistribution kinetics were investigated using $^{124}$I-cG250. Mice ($n = 40$) were injected intravenously with 5 MBq $^{124}$I-cG250 (25 $\mu$g) in 200 ml PBS on day 0. Groups of mice ($n = 5$) with a mean ($\pm$SD) tumor volume of 629 $\pm$ 195 $mm^3$ were sacrificed on day 0 (2 hours), 1, 2, 3, 5, 7, 10, and 14 after injection of radiolabeled antibody. Control mice ($n = 10$) in groups ($n = 5$) bearing SK-RC-52 xenografts received a single injection of radiolabeled $^{124}$I-huA33 on the same day, and were sacrificed on days 0 (2 hours) and 3.

Mice were sacrificed after having invasive oxygen measurements and in most cases PET imaging (both outlined previously) by exposure to sevofluorane. Mice were bled via cardiac puncture, and blood was collected into heparinized tubes. Tumors and organs (skin, liver, spleen, intestine, stomach, kidneys, brain, bone [femur], lungs, and heart) were immediately removed, blotted dry, and weighed (Sartorius Basic Balance, Ratingen, Germany). All samples

were counted in a dual chamber γ scintillation counter using a dual tracer program with standard windows set for the isotope as described previously [22,35].

### 2.10. Autoradiography

Immediately after sacrifice, an SK-RC-52 tumor from 1 mouse at time points 24, 48, 72, and 120 hours in the $^{124}$I biodistribution study was excised, frozen, and sectioned on a cryomicrotome (Zeis Microm HM 5000; Melbourne, Australia). Sequential 5-mm sections were used for direct autoradiography and for H and E staining. Tissue sections were placed on silane-coated glass slides and allowed to dry. Glass slides were placed face down in contact with standard radiography film. The glass slides and film were enclosed in a cassette and stored at −80°C. Slides and film were taken up at varying time intervals, and film was developed in a standard automatic film processor.

#### 2.10.1. Histology and immunohistochemistry

Immunohistochemistry was performed to confirm the presence and distribution of CAIX receptor in tumor xenografts. Selected xenografts (including all of day 0 and day 14 samples) were surgically removed, embedded in Tissue-Tek OCT compound (Diagnostic Division, Elkhart, IN), and cut at 5-μm thickness with a cryomicrotome. For CA IX staining, sections were incubated without antigen retrieval with rodent anti-CA IX (2.5 μg/ml; DAKO, Glostrup, Denmark) for 60 minutes at room temperature and subsequently developed with an avidin-biotin-peroxidase complex method (Envision system peroxidase mouse; DAKO) as previously described [39]. All sections were developed using diaminobenzidine, and subsequently counterstained with haematoxylin.

Semiquantitative analysis of stained xenografts was undertaken as previously described [40]. Tumor sections were initially scanned at ×25 magnification so that the distribution of staining could be assessed. At ×200 magnification, the sections were then analyzed field-by-field, from top left to bottom right of the section. Each field was assigned a % score of positive cells. Areas of necrosis, stroma, normal epithelium, and distinct edge effects were identified and not included in the analysis.

#### 2.10.2. Statistical analysis

Standard deviation and where appropriate standard error of the mean and 95% confidence intervals, linear correlation coefficients ($r^2$ 0.0 to 1.0) and *P* values were calculated with GraphPad Prism 4.0 software.

## 3. Results

### 3.1. In vitro properties of $^{124}$I-cG250

The radiolabeling efficiency (LE) for $^{124}$I-cG250 was 66.8% with a specific activity of 1.1 uCi/ug. For $^{124}$I-huA33, the LE was 52.2% and specific activity of 1.02 uCi/ug. After chromatographic purification, greater than 97% of $^{124}$I was bound to protein as determined by thin layer chromatography. Labeled antibody retained the ability to bind CAIX expressing cells (SK-RC-52) on flow cytometry, and immunoreactivity of 95%. Scatchard analysis of binding of $^{124}$I-cG250 to SK-RC-52 renal cell carcinoma cells determined the binding capacity of cells with the value to be $4 \times 10^5$ antibody molecules bound per cell. The apparent association constant ($K_a$) was also derived, giving a value of $2.18 \times 10^9$ $M^{-1}$. Serum stability of radioconjugate by thin-layer chromatographic analysis indicated 97%, 82%, and 81%, respectively, of $^{124}$I was bound to protein on days 0, 3, and 7. The immunoreactivity of $^{124}$I-cG250 in mouse serum incubated ex vivo at these times after injection was 95%, 81%, and 78%, respectively.

### 3.2. Oxygen tension measurement

The oxygen tension in normal tissue (muscle) was 35.08 ± 7.48 mmHg (mean ± SD) or 35.08 ± 2.41 mmHg (mean ± 95% CI), being significantly greater compared wth xenograft SK-RC-52 tumors at 5.02 ± 3.48 mmHg (mean ± SD) or 5.02 ± 1.12 mmHg (mean ± 95% CI) (Fig. 1). The tumor: normal tissue $pO_2$ ratio (mean ± 95% CI) for all tumors was 0.15:1.0 (±.03). The oxygen measurements (%; mean ± SD) for $HF_{2.5}$, $HF_5$, and $HF_{10}$ were 46 ± 30, 66 ± 0., and 83 ± 25 respectively for all tumors.

Comparing tumor volume to oxygen tension, a weak but significant inverse correlation was demonstrated ($r^2$ = 1133; $P$ = 0.04) but only when compared with $HF_{2.5}$ and not mean tumor $pO_2$, $HF_5$, or $HF_{10}$. Comparing the mean tumor $pO_2$ of the first group (day 0, $n$ = 5) with the last group (day 14, $n$ = 5), there was a trend toward reduced $pO_2$ (8.82 ± 4.65 and

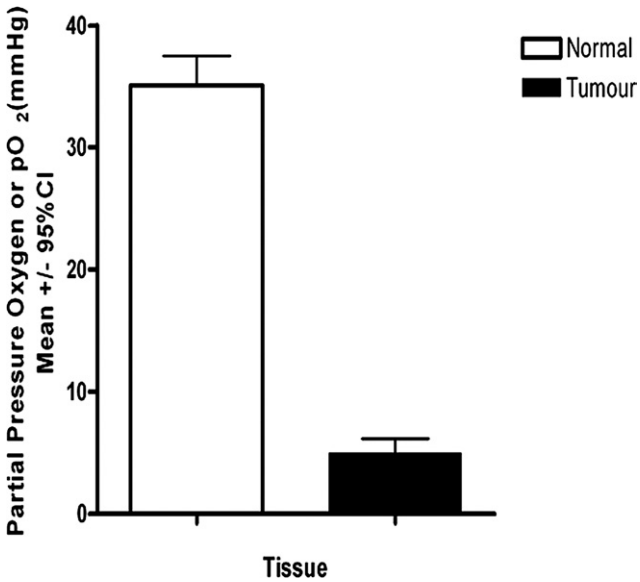


Fig. 1. Oxygen tension measurements in normal tissue and SK-RC-52 tumors (mean ± 95% CI) day 3 post injection.

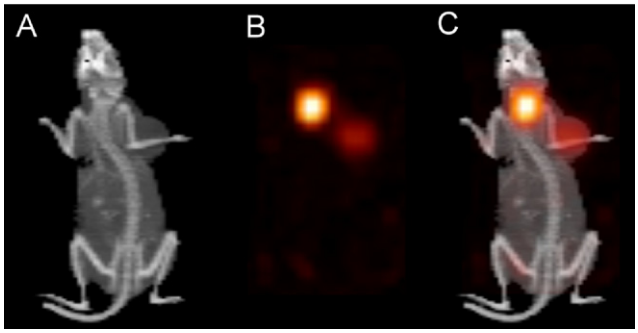


Fig. 2. PET/CT images of biodistribution of $^{124}$I-cG250 in SK-RC-52 xenografts in balb/c nude mouse day 3 postinjection. (A) 3D T demonstrates xenograft in right shoulder region; (B) $^{124}$I-cG250 PET scan demonstrates uptake in xenograft and some uptake in the thyroid; (C) Co-registered $^{124}$I-cG250 PET/CT image. (Color version of figure is available online.)

4.27± 1.62, respectively; mmHg, mean ± 95% CI) and a significant difference between $HF_{10}$ existed between groups (53.6 ± 31.12 and 91.2 ± 12.7 mmHg), respectively. With the same 2 groups from day 0 and 14, there was a trend toward increased tumor size over time (705.26 ± 204.99 and 586.69 ± 146.91 ($mm^3$), but this was not significant.

On the day of maximal $^{124}$I-cG250 uptake, day 3, there was a trend towards correlation between $pO_2$ and %ID/g on biodistribution, but this was not significant ($P = 0.08$).

### 3.3. Imaging

Localization of $^{124}$I-cG250 in BALB/c mice bearing SK-RC-52 xenograft as determined by PET/CT imaging was clearly apparent (Fig. 2). At 2 hours, some tumor localization was evident, with the images also showing cardiac blood pool activity. At 24 hours, there was definite localization of antibody to the CAIX-expressing xenograft. Over time, with decreasing blood pool activity, the uptake in the SK-RC-52 tumor was more clearly defined. There was a significant correlation between tumor uptake with SUVmean and SUVmax quantified by PET/CT and %/ID $^{124}$I-cG250, measured with a γ counter (Fig. 3).

### 3.4. Biodistribution

$^{124}$1-labeled biodistribution study results are presented in Table 1. One mouse died from the $^{124}$I-cG250 day 5 group (tumor embolus), leaving a total of 39 mice for analysis. The %ID/g of the isotope in SK-RC-52 xenografts peaked at 23.45 ± 5.07 (mean ± SD) 48 hours after antibody injection, and was maintained for a further 2 days (19.43 ± 4.31 and 10.64 ± 5.64 %ID/g, respectively). The tumor:blood ratio for $^{124}$I-labeled-cG250 was 4.94 ± 2.13 %ID/g on day 3 and reached 30.7 ± 21.7 %ID/g in SK-RC-52 on day 7 when blood clearance had occurred. The control antibody $^{124}$I-huA33 had very low tumor uptake (Table 1 and Fig. 4).

### 3.5. Pharmacokinetics

The calculated pharmacokinetic parameters for the 2-compartment model were: α half-life, 2.59 hours, β half-life, 40.5 hours; V1, 1.685 ml; C1, 0.08148 ml/h and serum area under curve, 65.8 ng*h/ml.

### 3.6. Histology, autoradiography, and immunohistochemistry

Hematoxylin staining indicated that the SK-RC-52 xenografts contained viable tissue peripherally, and a small amount in the center of the section, with variable areas of central necrosis and connective tissue (Fig. 5). Antigen (CAIX) was distributed evenly in areas corresponding to

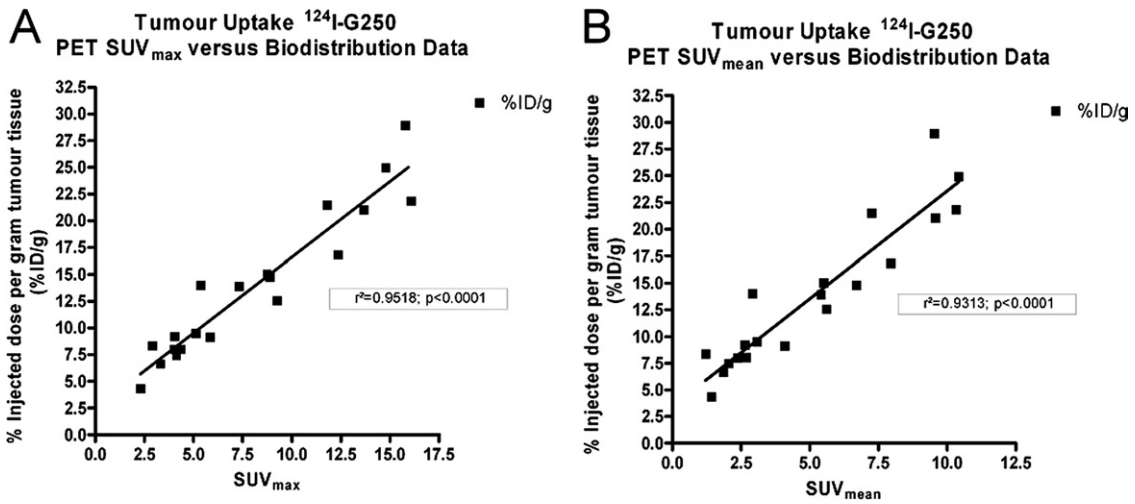


Fig. 3. Correlation between $^{124}$I-cG250 quantitative uptake inn SK-RC-52 xenografts as measured by $SUV_{max}$ and $SUV_{mean}$ from PET/CT studies and gamma well counting.

Table 1
Results of the biodistribution studies. The top half of the table represents the actual percentage of injected dose of radioisotope per gram of tissue. The bottom half summarises the tissue:blood ratio

| %Injected dose/gram tissue | $^{124}$I-cG250 | | | | Control $^{124}$I-huA33 | |
|---|---|---|---|---|---|---|
| | Day 0 | Day 2 | Day 3 | Day 7 | Day 0 | Day 3 |
| Blood | 32.2 ± 5.5 | 12.2 ± 4.3 | 4.8 ± 2.4 | 0.5 ± 0.5 | 48.5 ± 16.3 | 16.3 ± 3.7 |
| Tumor (SK-RC-52) | 9.6 ± 2.3 | 23.5 ± 5.1 | 19.4 ± 4.3 | 7.4 ± 1.8 | 5.7 ± 1.3 | 5.2 ± 0.6 |
| Liver | 10.9 ± 3.2 | 7.0 ± 2.2 | 3.4 ± 1.2 | 0.3 ± 0.2 | 8.8 ± 1.4 | 4.2 ± 1.0 |
| Kidney | 9.2 ± 2.6 | 3.29 ± 0.8 | 1.8 ± 0.8 | 0.2 ± 0.2 | 13.2 ± 1.6 | 5.9 ± 1.7 |
| Bone | 6.9 ± 6.8 | 2.16 ± 0.8 | 1.3 ± 0.5 | 0.1 ± 0.0 | 3.7 ± 1.1 | 2.4 ± 0.8 |
| Tissue/blood ratio | Day 0 | Day 2 | Day 3 | Day 7 | Day 0 | Day 3 |
| Tumor (SK-RC-52) | 0.3 ± 0.1 | 2.6 ± 2.2 | 4.9 ± 2.1 | 30.7 ± 21.7 | 0.13 ± 0.1 | 0.3 ± 0.1 |
| Liver | 0.3 ± 0.1 | 0.6 ± 0.2 | 0.9 ± 0.6 | 0.97 ± 0.6 | 0.19 ± 0.0 | 0.3 ± 0.0 |
| Kidney | 0.3 ± 0.0 | 0.30 ± 0.1 | 0.38 ± 0.0 | 0.60 ± 0.2 | 0.29 ± 0.1 | 0.4 ± 0.0 |
| Bone | 0.2 0.2 | 0.2 ± 0.0 | 0.27 ± 0.1 | 0.40 ± 0.4 | 0.1 ± 0.0 | 0.2 ± 0.0 |

viable tumor cells. Control slides for antigen staining showed no staining in the tumor itself.

$^{124}$I-cG250, assessed by autoradiography, was distributed throughout regions of viable tumor, including the central of tumors, with minimal activity in the necrotic areas (Fig. 5), indicating specific localization of radiolabeled cG250 to tumor cells. A similar distribution of $^{124}$I-cG250 throughout viable tumor cells was seen in all other time points studied (results not shown). On analysis of CAIX expression on days 0 vs. 14, there was a trend toward greater expression (61.27± 19.07 vs. 83.79 ± 8.75; %, mean ± 95% CI), but this was not significant. There was no significant correlation between $HP_{2.5}$ and CAIX expression for either day 0 ($P = 0.79$) or day 14 ($P = 0.33$) groups, nor was there for any other oxygen parameter (mean, $HP_5$, or $HP_{10}$).

## 4. Discussion

RCC is refractory to most current treatments when locally advanced or metastatic with more efficacious treatments required [1]. Noninvasive imaging of biologically relevant tumor markers with targeted monoclonal antibodies may provide for better imaging, staging, and treatment of tumors. Hypoxia in RCC has led to investigation of new imaging techniques that focus on proteins expressed in such environments. CAIX is expressed in numerous human malignancies [40,41], and is a significant molecular marker in RCC expressed in 87%–100% of clear cell RCC [42–44]. CAIX expression reflects significant changes in tumor biology, which may be used to predict clinical outcome and identify high-risk patients in need for adjuvant immunotherapy and CAIX-targeted therapies in RCC [45]. cG250 is a readily available monoclonal antibody that targets CAIX [22] Furthermore, extraordinarily high uptake and the requirement of a low dose to obtain tumor saturation with cG250 in patients with RCC make it an ideal antibody for tumor targeting and therapy [13,20,21,46,47]. Regarding therapy, monoclonal antibodies have the ability to destroy cancer cells with radiation or via immune effector function [20,21,47].

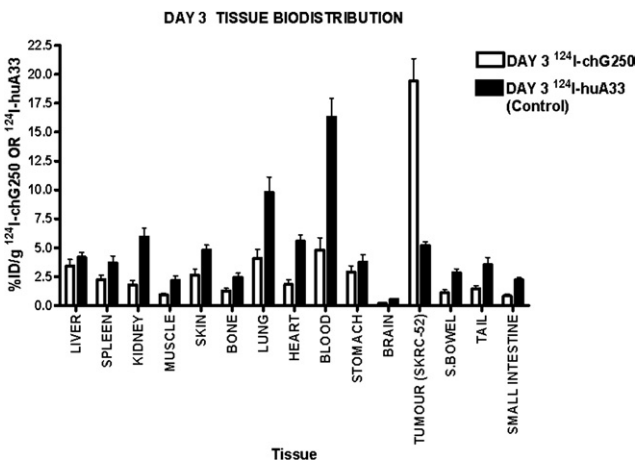


Fig. 4. Biodistribution data of $^{124}$I -cG250 and control $^{124}$I-c huA33G250 on day 3.

Various methods have been developed for assessing tumor hypoxia in xenograft tumor models and in patients. A drawback of many approaches is that they only allow assessment of tumor hypoxia at a single time point, as it is often necessary to remove the tumor or to sacrifice the animal at the time of hypoxia measurement [48]. Only few methods can be used for serial measurements of tumor hypoxia, including various direct oxygen sensing devices (e.g.m oxylite probe) and hypoxia imaging techniques, particularly using positron emission tomography [49,50]. However, the oxygen sensing devices, such as needle electrodes, can only access superficial tumors, and are highly dependent on the technical skill of the user [50]. Hence, noninvasive serial imaging would be ideal to replace not only electrode studies but also biodistribution studies that require animal sacrifice.

Characterization of intratumoral hypoxia in a human RCC xenograft model using invasive oxygen probe measurements was feasible. There have been no previous re-

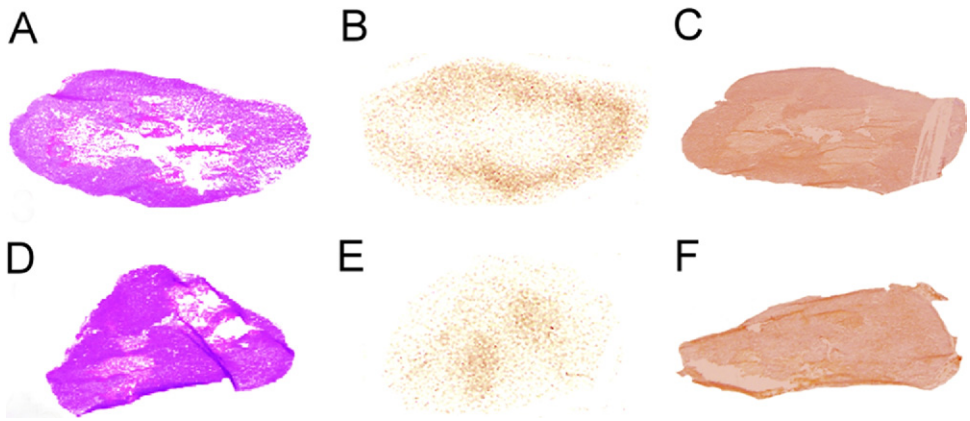


Fig. 5. Histology demonstrating (A) H and E tumor specimens from animals administered $^{124}$I -cG250 and sacrificed on days 3; (B) autoradiography of the same specimens in column (A) with dark areas representing high uptake of radiolabeled cG250 (the antibody binding CAIX); (C) CAIX expression assessed by immunohistochemistry. Comparative studies of a xenograft tumor from a mouse injected with control $^{124}$I-c huA33 (D) histology, (E) autoradiography, and (F) CAIX expression. (Color version of figure is available online.)

ports of oxygen measurements in a xenografted human RCC model, and results obtained support our initial reports of hypoxia within human RCC [19]. Oxygenation levels recorded (around 5 mmHg) were characteristic of an hypoxic tumor, and have been reported in tumors such as cervical cancer in the past [51]. Also, the tumors were heterogeneous with respect to individual measurements within each tumor, but the overall pattern was one of hypoxia, which has been demonstrated in other tumors [52]. The measurements in normal muscle were similar to those reported in the past (35–45 mmHg) [26]. The finding that an increased hypoxic fraction of cells was associated with increased tumor volume for all animals studied is not surprising, and has been reported in other xenograft tumor models [53]. As tumors grow larger, there is likely to be a greater proportion of hypoxic cell populations present because the tumor enlarges and requires angiogenesis to remain viable [52,54]. This was supported when comparing the groups from the first and last days of the study, where $HF_{10}$ (the number of measurements below 10 mmHg) increased to almost 100% over the 14 days, and this is compelling, as hypoxia is stated to be significant when oxygen tension is less than 10 mmHg [5].

Our second objective explored CAIX targeting with $^{124}$I-cG250 in nude mice with s.c. RCC xenografts, using biodistribution studies and PET/CT imaging. In summary, oxygen tension in the xenografts was low (5 mm Hg), CAIX expression was high, and the $^{124}$I-cG250 accumulated in the tumor (20%–25%ID/g, 2–3 days p.i.). Our primary purpose was to characterize the targeting of cG250 against CAIX using PET/CT. The relationship between G250 and CAIX is demonstrated by showing in PET/CT and autoradiography that both exist in viable tumor. Thus, $^{124}$I-cG250 targets and can quantitate CAIX expression in vivo. Although a recent report compared surrogate markers with PET/CT quantitation of $^{124}$I in animal models [55], our study represents a significant development because we have been able to delineate in an animal model a correlation between quantitative PET/CT and $\gamma$ well counting of antibody uptake in tumor tissue. The findings in this study create a potential alternative to the sacrifice of many animals to obtain quantitative data of uptake of compounds, such as radiolabeled monoclonal antibodies. Thus our findings have the ability to alter future experimentation methods once verified in future studies. The implications regarding cost, time, and, importantly, in the ethical treatment of animals are not insignificant [56].

We also further explored the relationship of cG250 uptake with hypoxia, and there was only a weak correlation between hypoxia and G250 uptake in a human RCC mouse model. Other studies have supported such a correlation [57,58]. In RCC, synthesis of CAIX is switched on by the loss of the tumor suppressor gene VHL [15], and is upregulated by HIF-1. CAIX is an attractive alternative intrinsic marker of hypoxia compared with HIF-1$\alpha$ because the protein is highly expressed on the cell surface and has a long half life in hypoxic tissue (unlike HIF-1$\alpha$) [17]. In our study, although CAIX expression was supported in this model, the level of expression could not be clearly related to hypoxia in the xenografted human RCC model. This may be due to small numbers and may also be related to the constitutive expression of CAIX in the SK-RC-52 cell line. This lends support to the theory that that CAIX expression is not necessarily a result of hypoxia in all circumstances, as cell lines may subvert traditional hypoxia mechanisms [59,60]. For example, one explanation is that in the earlier stages of tumor progression, noxious conditions, such as hypoxia or ischemia, induce CAIX expression as an adaptation to confer proliferation advantage for tumor growth and spread; however, when this malignant potential is attained in the later stages of tumor growth, continued CAIX expression is no longer a requirement [45]. Such theories also help to explain the variability of CAIX expression in relation to hypoxia, and that CAIX expression may be influenced by nonhypoxic stimuli [59,60].

## 5. Conclusion

Intratumoral hypoxia does exist within a human RCC xenograft model using invasive oxygen probe measurements. $^{124}$I-cG250 targets RCC with correlation between uptake on noninvasive PET-CT studies and traditional biodistribution studies, opening the possibility of using PET/CT in future studies. Finally, CAIX expression was not related to hypoxia in this model, supporting the hypothesis that cell lines may subvert known hypoxia mechanisms in hypoxic environments.

## Acknowledgments

The authors gratefully acknowledge the help and support of the staff of the PET Centre and the technical expertise of Dr. Carmel Murone, Ludwig Institute for Cancer Research at the Austin Hospital, Heidelberg, Victoria, Australia.

## References

[1] Linehan WM. Kidney cancer: Opportunity for disease specific targeted therapy. Urol Oncol 2008;26:542.
[2] Gray L, Conger AD, Eberr M, et al. Concentration of oxygen dissolved in tissues at the time of irradiation is a factor in radiotherapy. British Journal of Radiology 1953;26:638–48.
[3] Collingridge DR, Young WK, Vojnovic B, et al. Measurement of tumor oxygenation: A comparison between polarographic needle electrodes and a time-resolved luminescence-based optical sensor. Radiat Res 1997;147:329–34.
[4] Seddon BM, Honess DJ, Vojnovic B, et al. Measurement of tumor oxygenation: In vivo comparison of a luminescence fiber-optic sensor and a polarographic electrode in the p22 tumor. Radiat Res 2001; 155:837–46.
[5] Vaupel P, Kallinowski F, Okunieff P. Blood flow, oxygen and nutrient supply, and metabolic microenvironment of human tumors: A review. Cancer Res 1989;49:6449–65.
[6] Hockel M, Knoop C, Schlenger K, et al. Intratumoral $pO_2$ predicts survival in advanced cancer of the uterine cervix. Radiother Oncol 1993;26:45–50.
[7] Nordsmark M, Overgaard M, Overgaard J. Pretreatment oxygenation predicts radiation response in advanced squamous cell carcinoma of the head and neck. Radiother Oncol 1996;41:31–9.
[8] Nordsmark M, Bentzen SM, Rudat V, et al. Prognostic value of tumor oxygenation in 397 head and neck tumors after primary radiation therapy. An international multi-center study Radiother Oncol 2005; 77:18–24.
[9] Brizel DM, Scully SP, Harrelson JM, et al. Tumor oxygenation predicts for the likelihood of distant metastases in human soft tissue sarcoma. Cancer Res 1996;56:941–3.
[10] Shweiki D, Itin A, Soffer D, et al. Vascular endothelial growth factor induced by hypoxia may mediate hypoxia-initiated angiogenesis. Nature 1992;359:843–5.
[11] Fang J, Yan L, Shing Y, et al. HIF-1$\alpha$-mediated up-regulation of vascular endothelial growth factor, independent of basic fibroblast growth factor, is important in the switch to the angiogenic phenotype during early tumorigenesis. Cancer Res 2001;61:5731–5.
[12] Grabmaier K, Vissers JL, De Weijert MC, et al. Molecular cloning and immunogenicity of renal cell carcinoma-associated antigen G250. Int J Cancer 2000;85:865–70.
[13] Lam JS, Pantuck AJ, Belldegrun AS, et al. G250: A Carbonic Anhydrase IX Monoclonal Antibody. Curr Oncol Rep 2005;7:109–15.
[14] Grabmaier K, MC AdW, Verhaegh GW, et al. Strict regulation of CAIX(G250/MN) by HIF-1$\alpha$ in clear cell renal cell carcinoma. Oncogene 2004;23:5624–31.
[15] Závada J, Závadová Z, Zat'ovicova M, et al. Soluble form of carbonic anhydrase IX (CA IX) in the serum and urine of renal carcinoma patients. Br J Cancer 2003;89:1067–71.
[16] Chia SK, Wykoff CC, Watson PH, et al. Prognostic significance of a novel hypoxia-regulated marker, carbonic anhydrase IX, in invasive breast carcinoma. J Clin Oncol 2001;19:3660–8.
[17] Loncaster JA, Harris AL, Davidson SE, et al. Carbonic anhydrase (CA IX) expression, a potential new intrinsic marker of hypoxia: Correlations with tumor oxygen measurements and prognosis in locally advanced carcinoma of the cervix. Cancer Res 2001;61:6394–9.
[18] Giatromanolaki A, Koukourakis MI, Sivridis E, et al. Expression of hypoxia-inducible carbonic anhydrase-9 relates to angiogenic pathways and independently to poor outcome in non-small cell lung cancer. Cancer Res 2001;61:7992–8.
[19] Lawrentschuk N, Poon AM, Foo SS, et al. Assessing regional hypoxia in human renal tumors using 18F-fluoromisonidazole positron emission tomography. BJU Int 2005;96:540–6.
[20] Oosterwijk E, Debruyne FM. Radiolabeled monoclonal antibody G250 in renal-cell carcinoma. World J Urol 1995;13:186–90.
[21] Steffens MG, Boerman OC, Oosterwijk-Wakka JC, et al. Targeting of renal cell carcinoma with iodine-131-labeled chimeric monoclonal antibody G250. J Clin Oncol 1997;15:1529–37.
[22] Liu Z, Smyth FE, Renner C, et al. Anti-renal cell carcinoma chimeric antibody G250: Cytokine enhancement of in vitro antibody-dependent cellular cytotoxicity. Cancer Immunol Immunother 2002;51: 171–7.
[23] Oosterwijk E, Ruiter DJ, Hoedemaeker PJ, et al. Monoclonal antibody G 250 recognizes a determinant present in renal-cell carcinoma and absent from normal kidney. Int J Cancer 1986;38:489–94.
[24] Divgi CR, Pandit-Taskar N, Jungbluth AA, et al. Preoperative characterization of clear-cell renal carcinoma using iodine-124-labeled antibody chimeric G250 (124I-cG250) and PET in patients with renal masses: A phase I trial. Lancet Oncol 2007;8:304–10.
[25] Divgi C. Editorial: What ails solid tumor radioimmunotherapy? Cancer Biother Radiopharm 2006;21:81–4.
[26] Ziemer LS, Lee WMF, Vinogradov SA, et al. Oxygen distribution in murine tumors: Characterization using oxygen-dependent quenching of phosphorescence. J Appl Physiol 2005;98:1503–10.
[27] Scott AM, Lee FT, Jones R, et al. A phase I trial of humanized monoclonal antibody A33 in patients with colorectal carcinoma: Biodistribution, pharmacokinetics, and quantitative tumor uptake. Clin Cancer Res 2005;11:4810–7.
[28] Rosendahl AH, Forsberg G. IGF-I and IGFBP-3 augment transforming growth factor-$\beta$ actions in human renal carcinoma cells. Kidney Int 2006;70:1584–90.
[29] Lee FT, Hall C, Rigopoulos A, et al. Immuno-PET of human colon xenograft- bearing BALB/c nude mice using 124I-CDR-grafted humanized A33 monoclonal antibody. J Nucl Med 2001;42:764–9.
[30] Nikula TK, Curcio MJ, Brechbiel MW, et al. A rapid, single vessel method for preparation of clinical grade ligand conjugated monoclonal antibodies. Nucl Med Biol 1995;22:387–90.
[31] Lindmo T, Boven E, Cuttitta F, et al. Determination of the immunoreactive fraction of radiolabeled monoclonal antibodies by linear extrapolation to binding at infinite antigen excess. J Immunol Methods 1984;72:77–89.
[32] Tahtis K, Lee FT, Smyth FE, et al. Biodistribution properties of (111)indium-labeled C-functionalized trans-cyclohexyl diethylenetriaminepentaacetic acid humanized 3S193 diabody and F(ab′)(2) constructs in a breast carcinoma xenograft model. Clin Cancer Res 2001;7:1061–72.

[33] Lim DJ, Liu XL, Sutkowski DM, et al. Growth of an androgen-sensitive human prostate cancer cell line, LNCaP, in nude mice Prostate 1993;22:109–18.
[34] Beniers AJ, Peelen WP, Schaafsma HE, et al. Establishment and characterization of five new human renal tumor xenografts. Am J Pathol 1992;140:483–95.
[35] Clarke K, Lee FT, Brechbiel MW, et al. Therapeutic efficacy of anti-Lewis (y) humanized 3S193 radioimmunotherapy in a breast cancer model: Enhanced activity when combined with taxol chemotherapy. Clin Cancer Res 2000;6:3621–8.
[36] Urano M, Chen Y, Humm J, et al. Measurements of tumor tissue oxygen tension using a time-resolved luminescence-based optical oxylite probe: Comparison with a paired survival assay. Radiat Res 2002;158:167–73.
[37] Brurberg KG, Graff BA, Rofstad EK. Temporal heterogeneity in oxygen tension in human melanoma xenografts. Br J Cancer 2003; 89:350–6.
[38] Oxford Optronix Ltd. OxyLab pO2™, OxyLab LDF™: Advanced, Tissue Oxygenation and Blood Flow Monitoring Manual. Oxford, UK, 2004;1–4.
[39] Fillies T, Werkmeister R, van Diest PJ, et al. HIF1-$\alpha$ overexpression indicates a good prognosis in early stage squamous cell carcinomas of the oral floor. BMC Cancer 2005;5:84.
[40] Airley RE, Loncaster J, Raleigh JA, et al. GLUT-1 and CAIX as intrinsic markers of hypoxia in carcinoma of the cervix: Relationship to pimonidazole binding. Int J Cancer 2003;104:85–91.
[41] Ivanov S, Liao SY, Ivanova A, et al. Expression of hypoxia-inducible cell-surface transmembrane carbonic anhydrases in human cancer. Am J Pathol 2001;158:905–19.
[42] Uemura H, Nakagawa Y, Yoshida K, et al. MN/CA IX/G250 as a potential target for immunotherapy of renal cell carcinomas. Br J Cancer 1999;81:741–6.
[43] Liao SY, Aurelio ON, Jan K, et al. Identification of the MN/CA9 protein as a reliable diagnostic biomarker of clear cell carcinoma of the kidney. Cancer Res 1997;57:2827–31.
[44] Murakami Y, Kanda K, Tsuji M, et al. MN/CA9 gene expression as a potential biomarker in renal cell carcinoma. BJU Int 1999;83: 743–7.
[45] Bui MH, Seligson D, Han KR, et al. Carbonic anhydrase IX is an independent predictor of survival in advanced renal clear cell carcinoma: Implications for prognosis and therapy. Clin Cancer Res 2003; 9:802–11.
[46] Divgi CR, Bander NH, Scott AM, et al. Phase I/II radioimmunotherapy trial with iodine-131-labeled monoclonal antibody G250 in metastatic renal cell carcinoma. Clin Cancer Res 1998;4:2729–39.
[47] Steffens MG, Boerman OC, de Mulder PH, et al. Phase I radioimmunotherapy of metastatic renal cell carcinoma with 131I-labeled chimeric monoclonal antibody G250. Clin Cancer Res 1999;5:3268s–74s.
[48] Nelson DW, Cao H, Zhu Y, et al. A noninvasive approach for assessing tumor hypoxia in xenografts: Developing a urinary marker for hypoxia. Cancer Res 2005;65:6151–8.
[49] Foo SS, Abbott DF, Lawrentschuk N, et al. Functional imaging of intratumoral hypoxia. Mol Imaging Biol 2004;6:291–305.
[50] Brown JM, Le QT. Tumor hypoxia is important in radiotherapy, but how should we measure it? Int J Radiat Oncol Biol Phys 2002;54: 1299–301.
[51] Fyles AW, Milosevic M, Wong R, et al. Oxygenation predicts radiation response and survival in patients with cervix cancer. Radiother Oncol 1998;48:149–56.
[52] Schneider BP, Miller KD. Angiogenesis of breast cancer. J Clin Oncol 2005;23:1782–90.
[53] Saitoh J, Sakurai H, Suzuki Y, et al. Correlations between in vivo tumor weight, oxygen pressure, 31P NMR spectroscopy, hypoxic microenvironment marking by $\beta$-D-iodinated azomycin galactopyranoside ($\beta$-D-IAZGP), and radiation sensitivity. Int J Radiat Oncol Biol Phys 2002;54:903–9.
[54] Vaupel P, Hockel M. Tumor oxygenation and its relevance to tumor physiology and treatment. Adv Exp Med Biol 2003;510:45–9.
[55] Gonzalez Trotter DE, Manjeshwar RM, Doss M, et al. Quantitation of small-animal (124)I activity distributions using a clinical PET/CT scanner. J Nucl Med 2004;45:1237–44.
[56] Thomas D. Laboratory animals and the art of empathy. J Med Ethics 2005;31:197–202.
[57] Tan EY, Yan M, Campo L, et al. The key hypoxia regulated gene CAIX is up-regulated in basal-like breast tumors and is associated with resistance to chemotherapy. Br J Cancer 2009;100:405–11.
[58] Esbaugh AJ, Perry SF, Gilmour KM. Hypoxia-inducible carbonic anhydrase IX expression is insufficient to alleviate intracellular metabolic acidosis in the muscle of zebrafish, *Danio rerio*. Am J Physiol Regul Integr Comp Physiol 2009;296:R150–60.
[59] Nordsmark M, Eriksen JG, Gebski V, et al. Differential risk assessments from five hypoxia specific assays: The basis for biologically adapted individualized radiotherapy in advanced head and neck cancer patients. Radiother Oncol 2007;83:389–97.
[60] Vordermark D, Kaffer A, Riedl S, et al. Characterization of carbonic anhydrase IX (CA IX) as an endogenous marker of chronic hypoxia in live human tumor cells. Int J Radiat Oncol Biol Phys 2005;61: 1197–207.